Chemistry–A European Journal

Supporting Information

Quest for the Most Aromatic Pathway in Charged Expanded Porphyrins

Irene Casademont-Reig, Tatiana Woller, Victor García, Julia Contreras-García, William Tiznado, Miquel Torrent-Sucarrat,* Eduard Matito,* and Mercedes Alonso*

1 Conformational and topological switches induced by (de)protonation

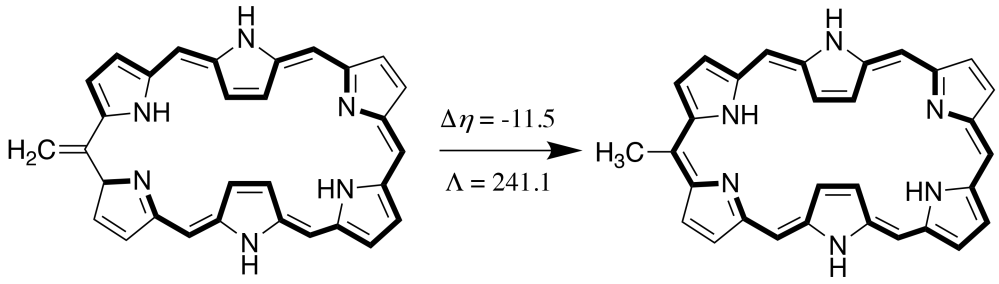

Figure S1: Reaction used to evaluate several global aromaticity descriptors in hexaphyrins. $\Delta\eta$ is given in kcal·mol^{-1} and Λ in ppm·cgs.

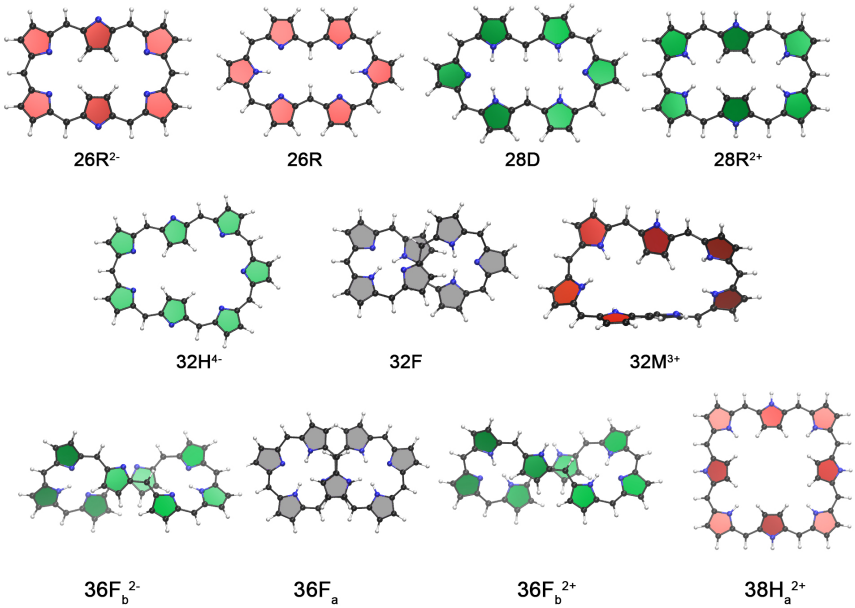

Figure S2: Lowest-energy conformations for neutral and charged hexa-, hepta-, and octaphyrins. Aromatic and antiaromatic macrocycles are colored as red and green, respectively. Nonaromatic macrocycles are colored in grey.

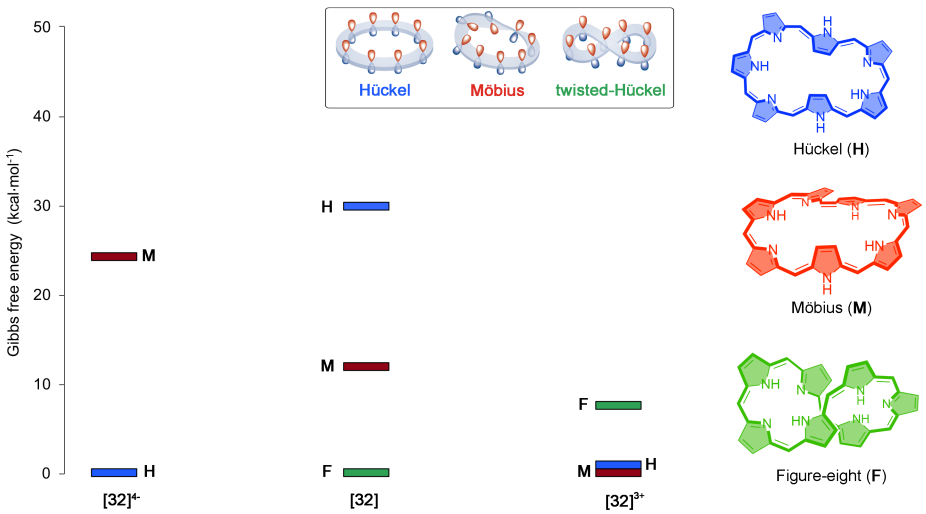

Figure S3: Evolution of the relative Gibbs free energy of selected heptaphyrins with oxidation state upon protonation or deprotonation of the macrocycles.

Table S1: Relative Gibbs free energies (kcal·mol^{-1}), hydrogen bond index (N_H) and ring strain (Φ_p in °) of hexaphyrins and heptaphyrins.[a]

[26]	ΔG	N_H	Φ_p	[28]	ΔG	N_H	Φ_p	[32]	ΔG	N_H	Φ_p
F	17.9	3	33.4	**F**	8.8	3	25.3	**F**	0.0	3.5	19.0
M	21.5	2	32.6	**M**	5.9	2.5	32.5	**M**	11.9	3	34.6
R	7.6	2	12.6	**R**	7.6	2	11.0	**H**	29.8	1	24.8
D	0.0	3	3.1	**D**	0.0	3	11.2	$\mathbf{F}^{4-}$	-	-	-
T	27.8	0	26.4	**T**	28.7	0	24.1	$\mathbf{M}^{4-}$	24.2	0	28.8
$\mathbf{F}^{2-}$	50.3	0	37.1	$\mathbf{F}^{2+}$	-	-	-	$\mathbf{H}^{4-}$	0.0	0	0.0
$\mathbf{M}^{2-}$	-	0	-	$\mathbf{M}^{2+}$	3.8	0	34.4	$\mathbf{F}^{3+}$	7.5	0	31.2
$\mathbf{R}^{2-}$	0.0	0	6.4	$\mathbf{R}^{2+}$	0.0	0	17.6	$\mathbf{M}^{3+}$	0.0	0	34.7
$\mathbf{D}^{2-}$	27.7	0	0.0	$\mathbf{D}^{2+}$	8.1	0	16.3	$\mathbf{H}^{3+}$	0.8	0	24.8
$\mathbf{T}^{2-}$	7.1	0	24.4	$\mathbf{T}^{2+}$	9.5	0	32.8				

[a] Gibbs free energies at the M06-2X/6-311+G(d,p)//CAM-B3LYP/6-311G(d,p) level of theory.

Table S2: Relative Gibbs free energies (kcal·mol^{-1}), hydrogen bond index (N_H) and ring strain (Φ_p in °) of octaphyrins.[a]

[36]	ΔG	N_H	Φ_p	[36]	ΔG	N_H	Φ_p	[38]	ΔG	N_H	Φ_p	[36]	ΔG	N_H	Φ_p
$\mathbf{F}_a$	0.0	4	15.4	$\mathbf{F}_a^{2-}$	12.6	3	15.1	$\mathbf{F}_a^{2+}$	2.3	0	17.7	$\mathbf{F}_a^{2+}$	1.5	3	16.0
$\mathbf{F}_b$	14.5	3	17.7	$\mathbf{F}_b^{2-}$	0.0	3	20.1	$\mathbf{F}_b^{2+}$	9.7	0	24.7	$\mathbf{F}_b^{2+}$	0.0	3	19.8
$\mathbf{M}_a$	27.9	2.5	24.5	$\mathbf{M}_a^{2-}$	1.2	2.5	23.8	$\mathbf{M}_a^{2+}$	10.9	0	26.4	$\mathbf{M}_a^{2+}$	4.6	2	24.8
$\mathbf{M}_b$	49.7	0	30.1	$\mathbf{M}_b^{2-}$	21.4	0	31.2	$\mathbf{M}_b^{2+}$	11.0	0	35.8	$\mathbf{M}_b^{2+}$	27.9	0	31.0
$\mathbf{H}_a$	33.4	0	6.0	$\mathbf{H}_a^{2-}$	12.2	0	3.8	$\mathbf{H}_a^{2+}$	0.0	0	16.7	$\mathbf{H}_a^{2+}$	13.7	0	11.1
$\mathbf{H}_b$	49.8	0	26.7	$\mathbf{H}_b^{2-}$	17.4	0	22.1	$\mathbf{H}_b^{2+}$	5.8	0	27.8	$\mathbf{H}_b^{2+}$	31.6	0	27.6

[a] Gibbs free energies at the M06-2X/6-311+G(d,p)//CAM-B3LYP/6-311G(d,p) level of theory.

Table S3: Relative Gibbs free energies (kcal·mol^{-1}) and RMSD values of expanded porphyrins optimized with CAM-B3LYP and different basis sets.

system	ΔG D3 dispersion	ΔG No dispersion	RMSD	system	ΔG 6-311+G(d,p)	ΔG 6-311G(d,p)	RMSD
26R^{2-}	0	0	0.017	**28R**	9.9	7.6	0.008
26D^{2-}	26.9	27.7	0.030	**28D**	0	0	0.057
26F^{2-}	51.1	50.4	0.052	**28T**	30.2	28.7	0.011
26M^{2-}	5.5	7.1	0.026	**28M**	7.4	5.9	0.015
26M^{2-}	*a*	*a*	*a*	**28F**	10.3	8.8	0.017
28R^{2+}	0	0	0.107	**32F**$^{4-}$	*a*	*a*	*a*
28M^{2+}	3.5	3.8	0.143	**32H**$^{4-}$	0	0	0.017
28T^{2+}	9.8	9.5	0.022	**32M**$^{4-}$	22.8	24.2	0.018
28D^{2+}	7.7	8.1	0.043				
28F^{2+}	*a*	*a*	*a*				

[a] Those topologies could not be optimized as an energy minimum since the conformation changes upon the optimization.

Table S4: Pearson coefficients between several descriptors of aromaticity for unsubstituted expanded porphyrins (n=20).

	$\Delta\eta$	Λ	NICS(0)	NICS$_{zz}$(1)
$\Delta\eta$	1			
Λ	-0.672[a]	1		
NICS(0)	-0.641[a]	0.915[a]	1	
NICS$_{zz}$(1)	-0.670[a]	0.962[a]	0.923[a]	1

[a] The correlation is significant at the 0.01 level (two-tailed).

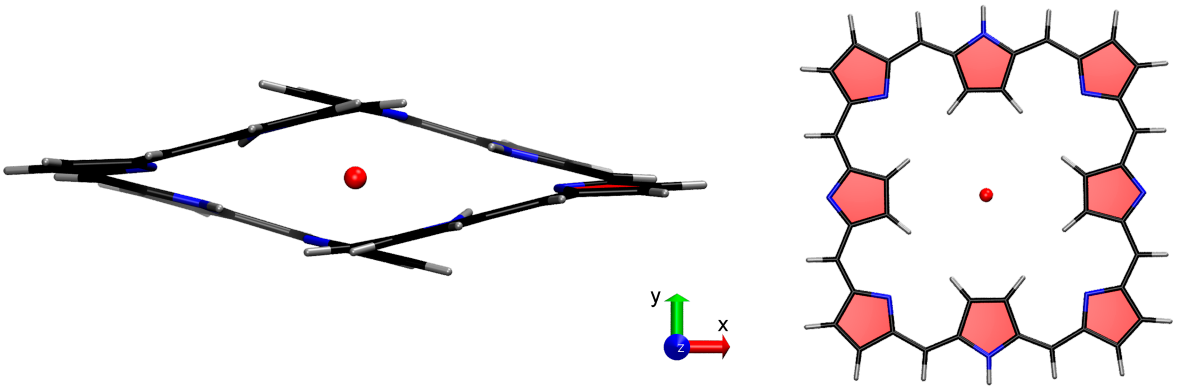

Figure S4: Orientation of the twisted-Hückel and Hückel octaphyrin structures employed in the calculation of the NICS-based indices. The magnetic field is oriented along the z axis.

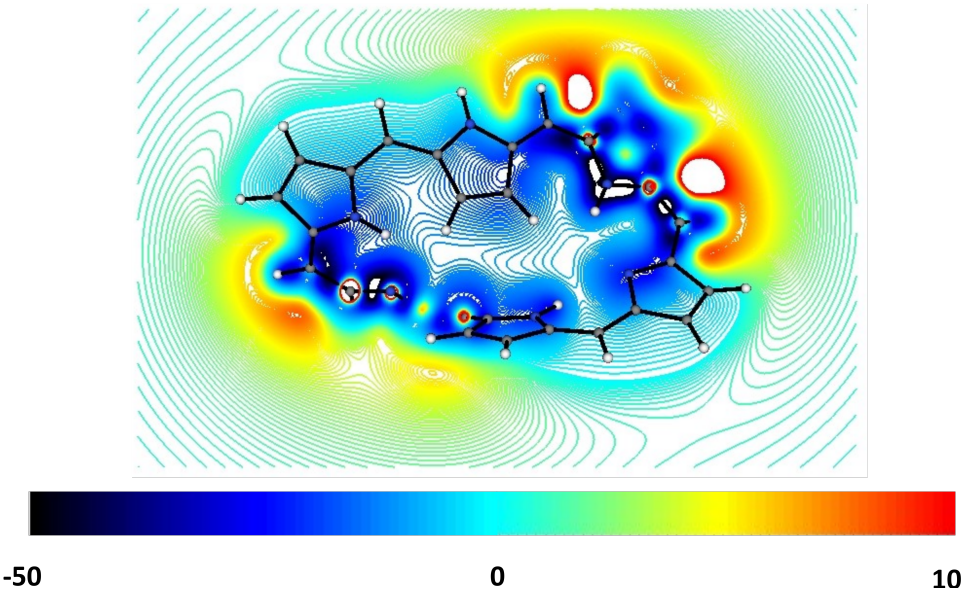

Figure S5: 2D-NICS$_{zz}$(1) plots (in ppm) of the magnetic shielding of **28M** in the xy plane 1Å situated above the molecular plane.

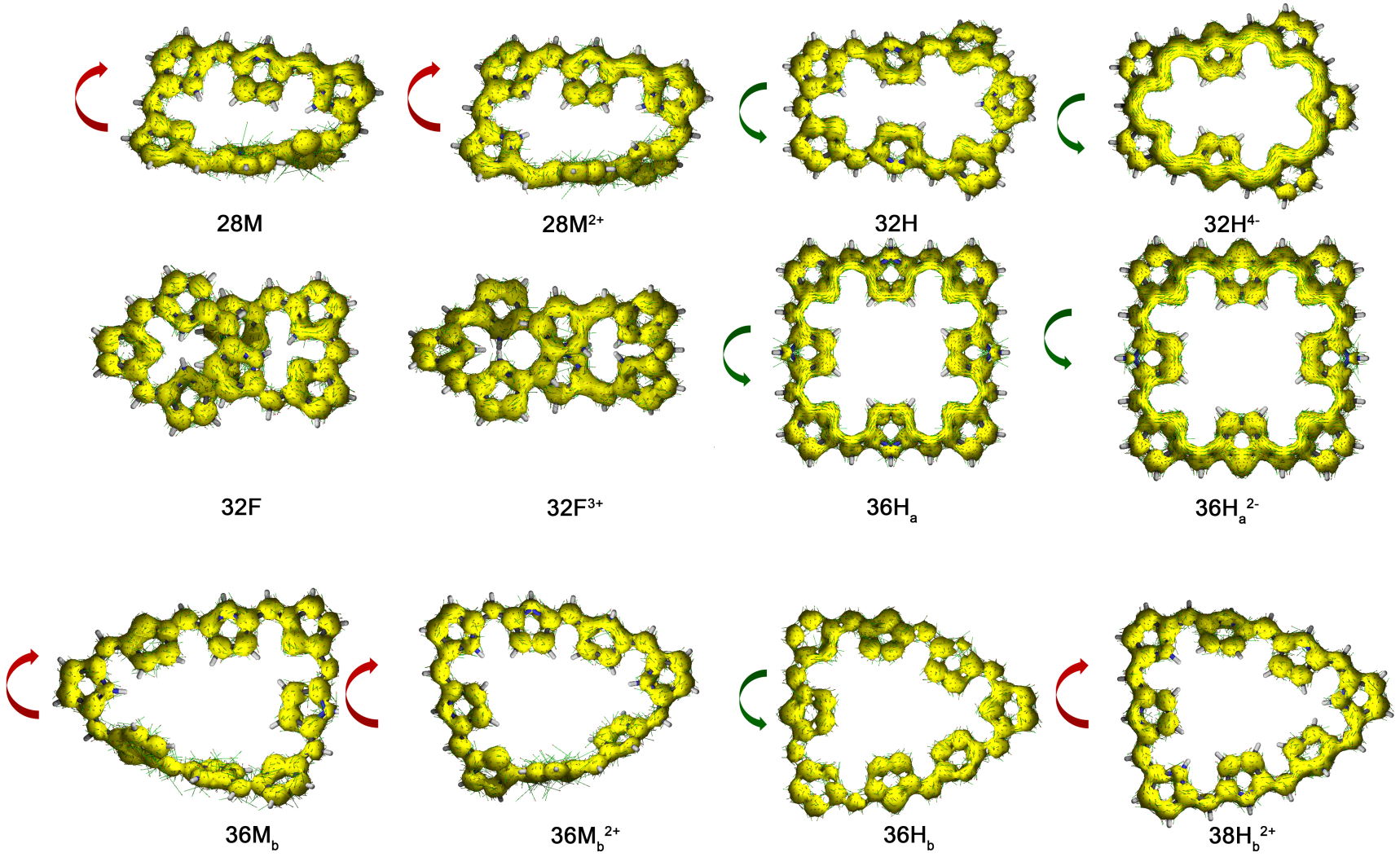

Figure S6: AICD plots of selected neutral, protonated, and deprotonated expanded porphyrins (**28M**, **28M**$^{2+}$, **32H**, **32H**$^{4-}$, **32F**, **32F**$^{3+}$, **36H**$_a$, **36H**$_a^{2-}$, **36M**$_b$, **36M**$_b^{2+}$, **36H**$_b$, and **38H**$_b^{2+}$) (isovalue of 0.06 au).

2 Magnetically induced currents in neutral and charged expanded porphyrins

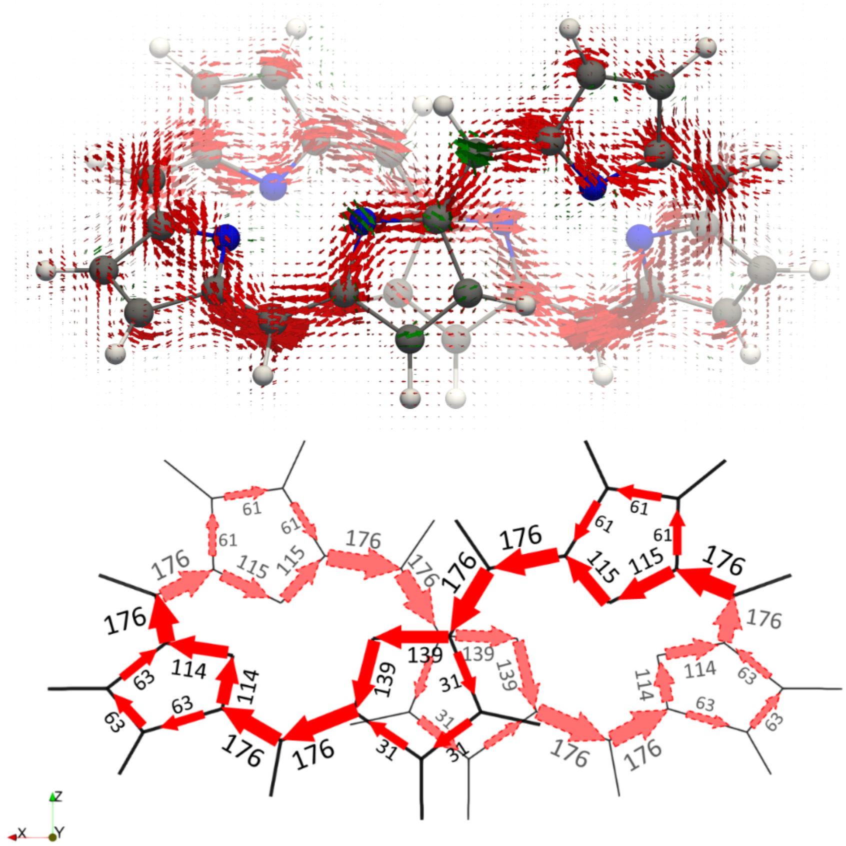

Figure S7: Visualization of the current density plots using a vector representation in $\mathbf{26F}^{2-}$. The percentage ratios are with respect to the net bond current strength in pyrrole (11.8 nA·T^{-1}). The external magnetic field is parallel to the symmetry z axis. The percentage ratios are with respect to the net bond current strength in pyrrole (11.8 nA·T^{-1}).

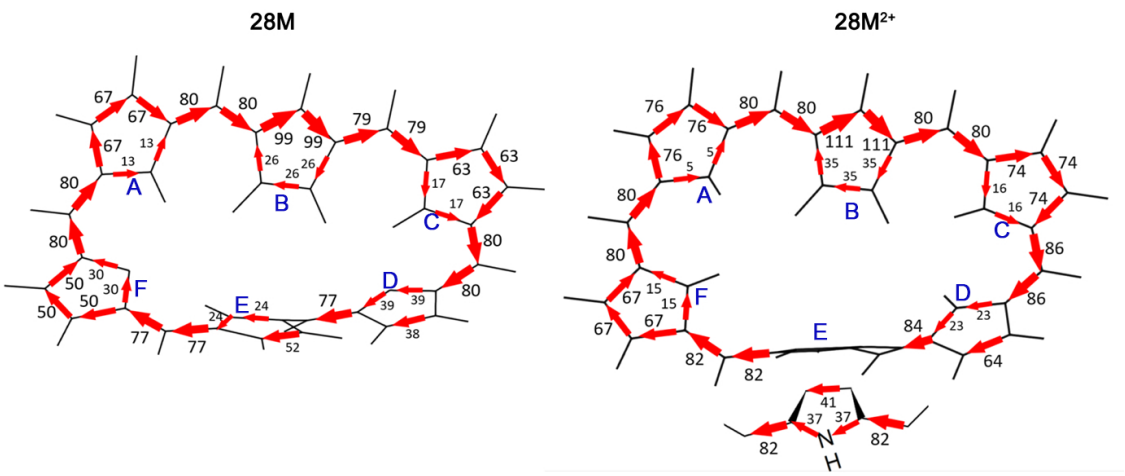

Figure S8: Percentage ratios of the current strength in **28M** and $\mathbf{28M}^{2+}$ with respect to the net bond current strength in pyrrole (11.8 nA·T^{-1}).

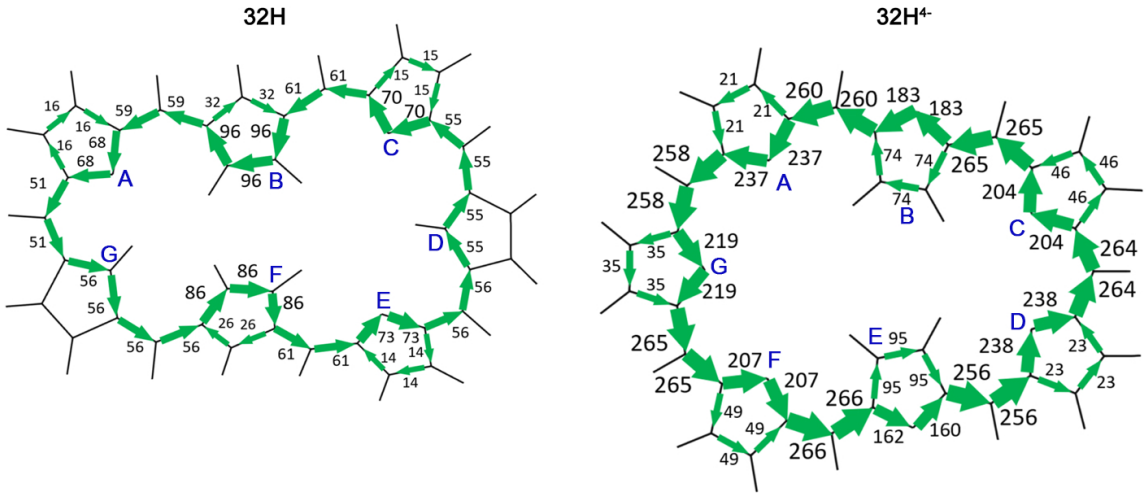

Figure S9: Percentage ratios of the current strength in **32H** and $\mathbf{32H}^{4-}$ with respect to the net bond current strength in pyrrole (11.8 nA·T^{-1}).

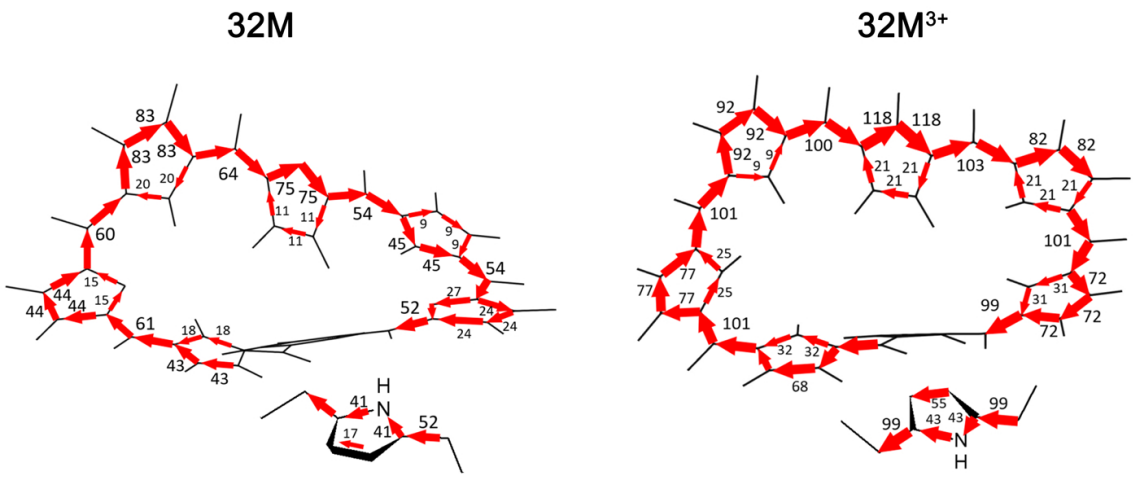

Figure S10: Percentage ratios of the current strength in **32M** and $\mathbf{32M}^{3+}$ with respect to the net bond current strength in pyrrole (11.8 nA·T^{-1}).

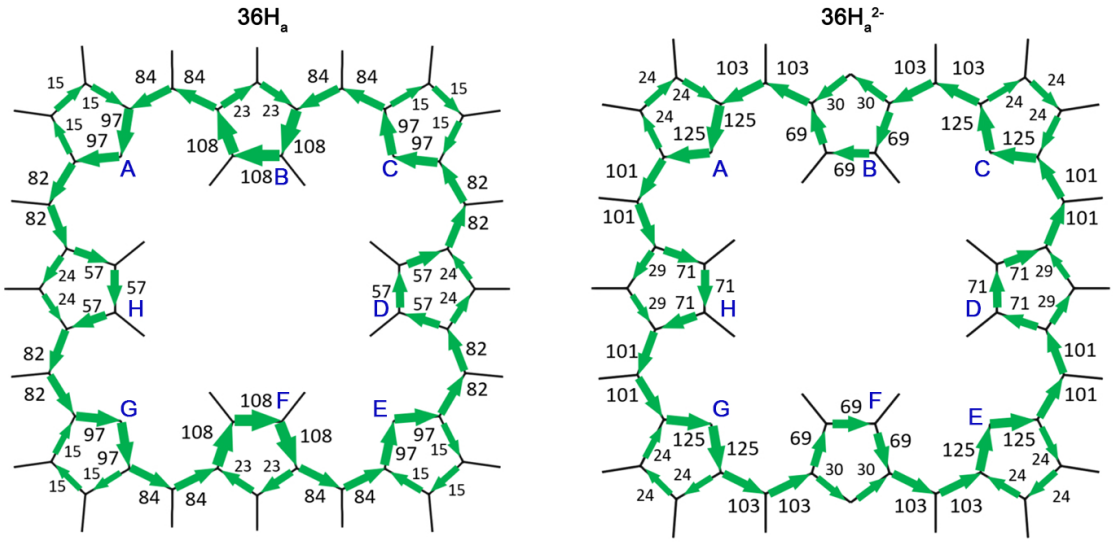

Figure S11: Percentage ratios of the current strength in $\mathbf{36H}_a$ and $\mathbf{36H}_a^{2-}$ with respect to the net bond current strength in pyrrole (11.8 nA·T^{-1}).

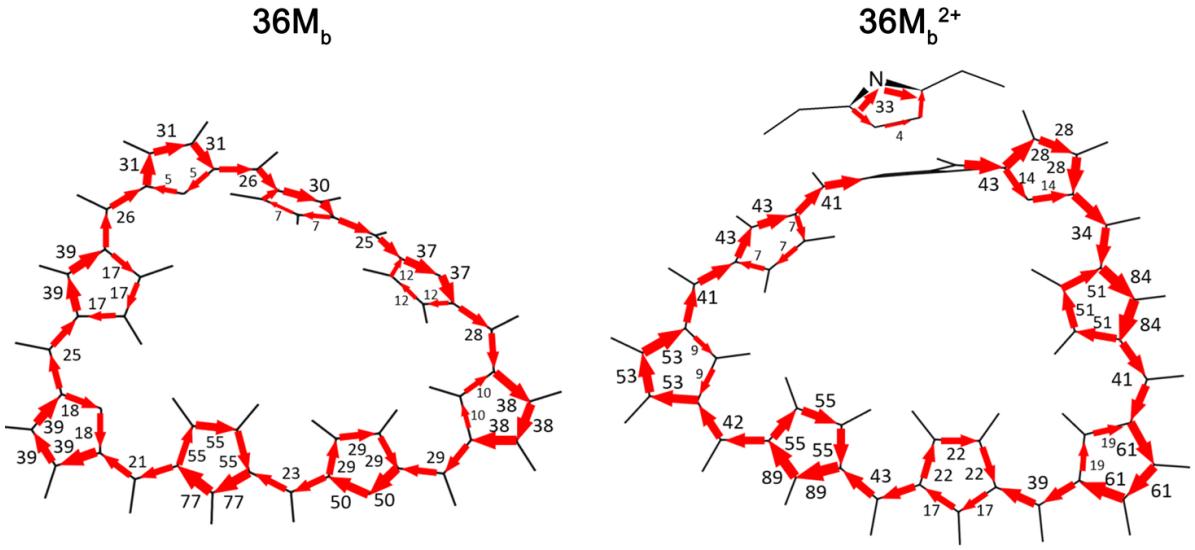

Figure S12: Percentage ratios of the current strength in **36M**$_b$ and **36M**$_b^{2+}$ with respect to the net bond current strength in pyrrole (11.8 nA·T^{-1}).

3 Local aromaticity indices in neutral and charged expanded porphyrins

Table S5: Evolution of the aromaticity indices for the annulene pathway of expanded porphyrins upon the protonation of the macrocycle.[a]

system	π e$^-$	FLU	BOA	HOMA	BLA	AV1245	AV$_{min}$
28R	28	0.021	0.300	0.620	0.067	1.31	0.42
28R^{2+}	28	0.020	0.264	0.682	0.051	1.07	0.16
28M	28	0.018	0.269	0.677	0.059	1.45	0.60
28M^{2+}	28	0.018	0.253	0.718	0.048	1.14	0.01
32F	32	0.020	0.292	0.632	0.065	1.28	0.39
32F^{3+}	32	0.020	0.251	0.695	0.048	1.15	0.15
32M	32	0.020	0.292	0.664	0.065	1.40	0.53
32M^{3+}	32	0.017	0.234	0.749	0.045	1.17	0.00
36M$_b$	36	0.025	0.330	0.582	0.076	1.16	0.35
36M$_b^{2+}$	38	0.024	0.313	0.593	0.069	1.48	0.15
36H$_b$	36	0.025	0.323	0.579	0.076	1.15	0.21
38H$_b^{2+}$	38	0.019	0.250	0.702	0.024	1.48	0.04

[a] All indices were calculated at the CAM-B3LYP/6-311+G(d,p) level of theory.

Table S6: Evolution of the aromaticity indices for the inner pathway of expanded porphyrins upon the protonation of the macrocycle.[a]

system	π e$^-$	FLU	BOA	HOMA	BLA	AV1245	AV$_{min}$
28R	24	0.020	0.251	0.719	0.054	0.07	0.03
28R^{2+}	24	0.020	0.219	0.735	0.043	-0.07	0.05
28M	24	0.016	0.215	0.784	0.043	0.13	0.01
28M^{2+}	24	0.019	0.217	0.750	0.041	-0.16	0.01
32F	28	0.017	0.238	0.759	0.053	0.38	0.02
32F^{3+}	28	0.020	0.227	0.732	0.044	0.11	0.10
32M	28	0.018	0.238	0.765	0.051	0.33	0.01
32M^{3+}	28	0.018	0.211	0.783	0.038	0.10	0.00
36M$_b$	32	0.024	0.287	0.662	0.064	0.43	0.04
36M$_b^{2+}$	32	0.022	0.259	0.701	0.057	0.16	0.03
36H$_b$	32	0.024	0.286	0.662	0.064	0.43	0.00
38H$_b^{2+}$	32	0.018	0.208	0.783	0.038	-0.34	0.02

[a] All indices were calculated at the CAM-B3LYP/6-311+G(d,p) level of theory.

Table S7: Evolution of the aromaticity indices for the outer pathway of expanded porphyrins upon the protonation of the macrocycle.[a]

system	π e$^-$	FLU	BOA	HOMA	BLA	AV1245	AV$_{min}$
28R	30	0.026	0.324	0.487	0.069	1.45	0.08
28R^{2+}	30	0.022	0.295	0.604	0.063	1.59	0.20
28M	30	0.024	0.311	0.515	0.067	1.48	0.04
28M^{2+}	30	0.020	0.283	0.642	0.059	1.67	0.22
32F	35	0.027	0.330	0.443	0.070	1.39	0.01
32F^{3+}	35	0.021	0.156	0.613	0.060	1.54	0.12
32M	35	0.026	0.324	0.475	0.069	1.41	0.06
32M^{3+}	35	0.019	0.267	0.684	0.055	1.63	0.20
36M$_b$	40	0.032	0.362	0.315	0.079	1.14	0.03
36M$_b^{2+}$	40	0.027	0.323	0.464	0.057	0.16	0.03
36H$_b$	40	0.032	0.363	0.300	0.080	1.12	0.02
38H$_b^{2+}$	40	0.019	0.003	0.665	0.000	1.87	0.27

[a] All indices were calculated at the CAM-B3LYP/6-311+G(d,p) level of theory.

Table S8: Evolution of the aromaticity indices for the annulene pathway of expanded porphyrins upon deprotonation of the macrocycles.[a]

system	π e$^-$	FLU	BOA	HOMA	BLA	AV1245	AV$_{min}$
26R	26	0.019	0.278	0.716	0.065	1.56	0.60
26R^{2-}	26	0.017	0.218	0.659	0.057	1.58	0.38
26F	26	0.023	0.317	0.619	0.074	1.27	0.35
26F^{2-}	26	0.015	0.124	0.720	0.044	1.66	0.66
32M	32	0.020	0.292	0.664	0.065	1.40	0.53
32M^{4-}	32	0.023	0.261	0.450	0.066	1.30	0.02
32H	32	0.022	0.309	0.611	0.070	1.21	0.42
32H^{4-}	32	0.024	0.280	0.423	0.071	1.11	0.01
36H$_a$	36	0.022	0.304	0.636	0.068	1.21	0.40
36H$_a^{2-}$	34	0.020	0.265	0.659	0.067	1.36	0.54

[a] All indices were calculated at the CAM-B3LYP/6-311+G(d,p) level of theory.

Table S9: Evolution of the aromaticity indices for the inner pathway of expanded porphyrins upon deprotonation.[a]

system	π e$^-$	FLU	BOA	HOMA	BLA	AV1245	AV$_{min}$
26R	24	0.017	0.250	0.785	0.057	1.05	0.12
26R^{2-}	24	0.009	0.142	0.888	0.045	1.73	1.23
26F	24	0.020	0.281	0.712	0.067	0.86	0.43
26F^{2-}	24	0.006	0.018	0.971	0.029	1.83	1.54
32M	28	0.018	0.238	0.765	0.051	0.33	0.01
32M^{4-}	28	0.010	0.137	0.840	0.044	0.86	0.21
32H	28	0.020	0.258	0.730	0.056	0.40	0.01
32H^{4-}	28	0.012	0.175	0.793	0.052	0.82	0.09
36H$_a$	32	0.020	0.260	0.738	0.056	0.56	0.03
36H$_a^{2-}$	32	0.017	0.219	0.773	0.049	0.93	0.11

[a] All indices were calculated at the CAM-B3LYP/6-311+G(d,p) level of theory.

Table S10: Evolution of the aromaticity indices for the outer pathway of expanded porphyrins upon deprotonation.[a]

system	π e$^-$	FLU	BOA	HOMA	BLA	AV1245	AV$_{min}$
26R	30	0.031	0.351	0.346	0.078	1.02	0.01
26R^{2-}	30	0.031	0.334	0.286	0.077	1.13	0.01
26F	30	0.034	0.369	0.256	0.080	1.00	0.00
26F^{2-}	30	0.029	0.296	0.345	0.069	1.25	0.18
32M	35	0.026	0.324	0.475	0.069	1.41	0.06
32M^{4-}	35	0.028	0.311	0.305	0.070	1.51	0.02
32H	35	0.029	0.348	0.389	0.077	1.25	0.01
32H^{4-}	35	0.029	0.322	0.280	0.072	1.47	0.01
36H$_a$	40	0.030	0.351	0.360	0.076	1.20	0.04
36H$_a^{2-}$	40	0.027	0.314	0.456	0.068	1.70	0.22

[a] All indices were calculated at the CAM-B3LYP/6-311+G(d,p) level of theory.

Table S11: Aromaticity indices of the three most delocalized circuits of anionic expanded porphyrins.[a]

system	Circuit[b]	π e$^-$	FLU	BOA	HOMA	BLA	AV1245	AV$_{min}$
26R^{2-}	iiiiii	24	0.009	0.142	0.888	0.045	1.73	1.23
26R^{2-}	iiiiio	25	0.012	0.167	0.812	0.047	1.78	0.59
26R^{2-}	oiiiio	26	0.015	0.19	0.741	0.048	1.82	0.59
26F^{2-}	iiiiii	24	0.006	0.018	0.971	0.029	1.83	1.53
26F^{2-}	iiiiio	25	0.010	0.074	0.841	0.037	1.74	0.66
26F^{2-}	iiioio	26	0.014	0.124	0.732	0.044	1.66	0.63
32H^{4-}	iooioio	32	0.021	0.26	0.503	0.060	1.16	0.19
32H^{4-}	ioiioio	31	0.021	0.256	0.516	0.064	0.96	0.19
32H^{4-}	ioiioii	30	0.021	0.254	0.531	0.068	0.73	0.19
32M^{4-}	oioooii	32	0.020	0.234	0.535	0.056	1.54	0.35
32M^{4-}	oioioio	32	0.019	0.23	0.543	0.055	1.53	0.35
32M^{4-}	oioioii	31	0.019	0.225	0.565	0.059	1.34	0.35
36H$_a^{2-}$	iiioiiio	34	0.020	0.265	0.659	0.067	1.36	0.54
36H$_a^{2-}$	iiioioio	35	0.021	0.284	0.628	0.068	1.29	0.54
36H$_a^{2-}$	ioioioio	36	0.023	0.302	0.599	0.069	1.23	0.54

[a] All indices were calculated at the CAM-B3LYP/6-311+G(d,p) level of theory.
[b] i denotes the inner route (C-N-C) and o the outer route (C-C) in a pyrrole ring. The labelling of the conjugation pathway starts from the top right five-membered ring.

Table S12: Aromaticity indices of the three most delocalized circuits of cationic expanded porphyrins.[a]

system	Circuit[b]	π e$^-$	FLU	BOA	HOMA	BLA	AV1245	AV$_{min}$
28R^{2+}	oooooo	30	0.022	0.295	0.604	0.063	1.59	0.20
28R^{2+}	iooooo	29	0.021	0.263	0.642	0.174	1.34	0.16
28M^{2+}	oooooo	30	0.020	0.283	0.642	0.059	1.67	0.22
28M^{2+}	ooiooo	29	0.019	0.266	0.685	0.052	1.46	0.20
32F^{3+}	iooooo	32	0.017	0.232	0.761	0.039	1.38	0.20
32F^{3+}	iooioo	33	0.018	0.25	0.713	0.045	1.38	0.21
32F^{3+}	iooooo	34	0.020	0.273	0.655	0.054	1.41	0.17
32M^{3+}	ooiiooi	32	0.016	0.222	0.787	0.036	1.25	0.28
32M^{3+}	oooiooi	33	0.017	0.235	0.760	0.042	1.43	0.32
32M^{3+}	oooiooo	34	0.018	0.252	0.724	0.049	1.52	0.24
36M$_b^{2+}$	ooooiio	38	0.024	0.313	0.593	0.069	1.48	0.15
36M$_b^{2+}$	ooooiiio	37	0.025	0.313	0.577	0.072	1.28	0.15
36M$_b^{2+}$	ooioiiio	36	0.021	0.285	0.674	0.060	1.12	0.12
38H$_b^{2+}$	oooooooo	40	0.019	0.266	0.665	0.055	1.87	0.27
38H$_b^{2+}$	oooioooo	39	0.018	0.249	0.716	0.048	1.73	0.21
38H$_b^{2+}$	ooooooio	39	0.018	0.249	0.708	0.048	1.71	0.19

[a] All indices were calculated at the CAM-B3LYP/6-311+G(d,p) level of theory.
[b] i denotes the inner route (C-N-C) and o the outer route (C-C). The labelling of the conjugation patway starts from the top right five-membered ring, except for 32M and 36M in which the first labelled five-membered ring corresponds to the top left one.

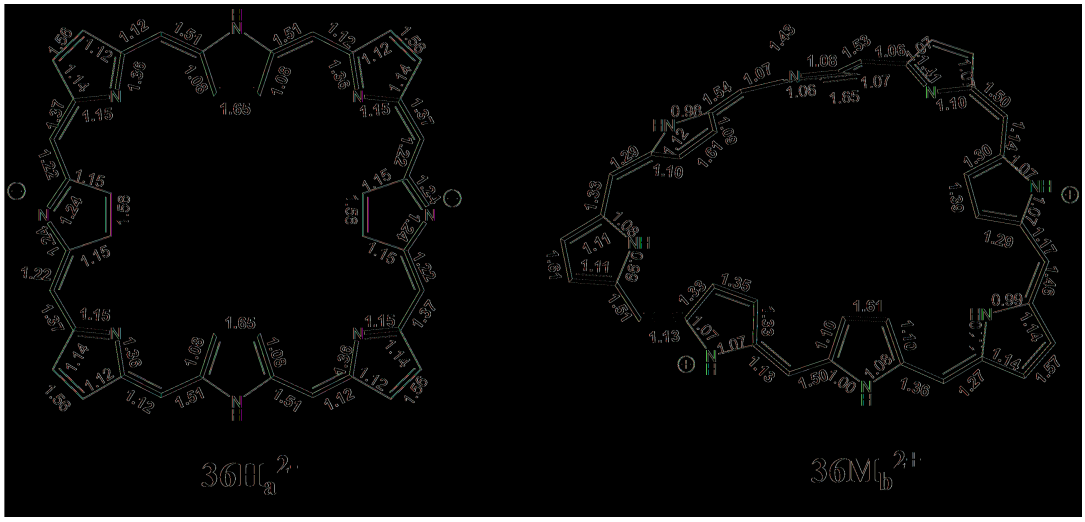

Figure S13: Delocalization indices (DIs) for $\mathbf{36H}_a^{2-}$ and $\mathbf{36M}_b^{2+}$ macrocycles computed at the CAM-B3LYP/6-311G(d,p) level of theory. The main conjugation pathway is depicted with bold bonds.

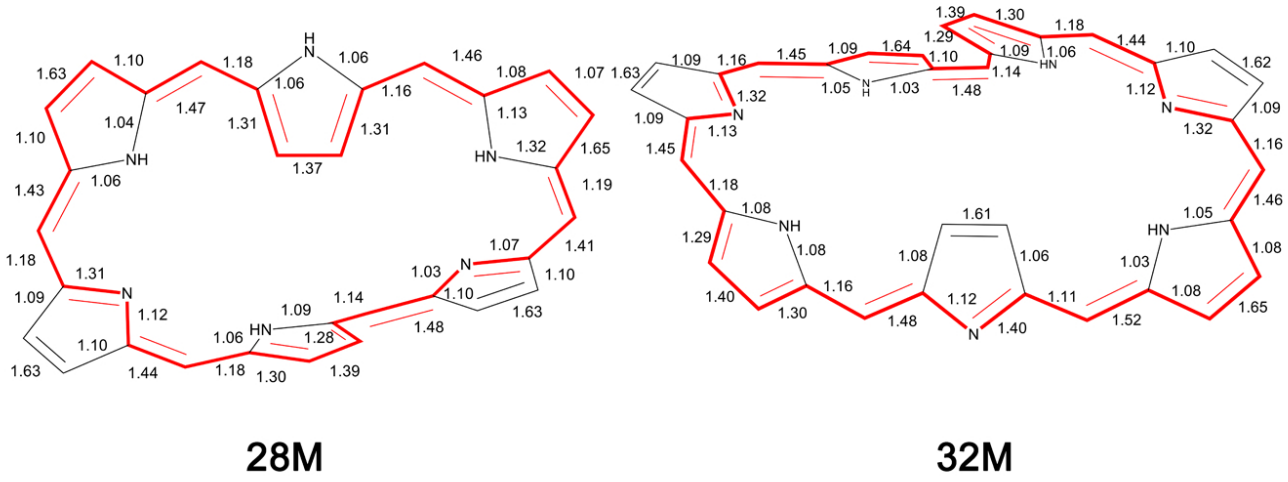

Figure S14: Delocalization indices (DIs) for **28M** and **32M** macrocycles computed at the CAM-B3LYP/6-311G(d,p) level of theory. The main conjugation pathway is depicted with bold red bonds.

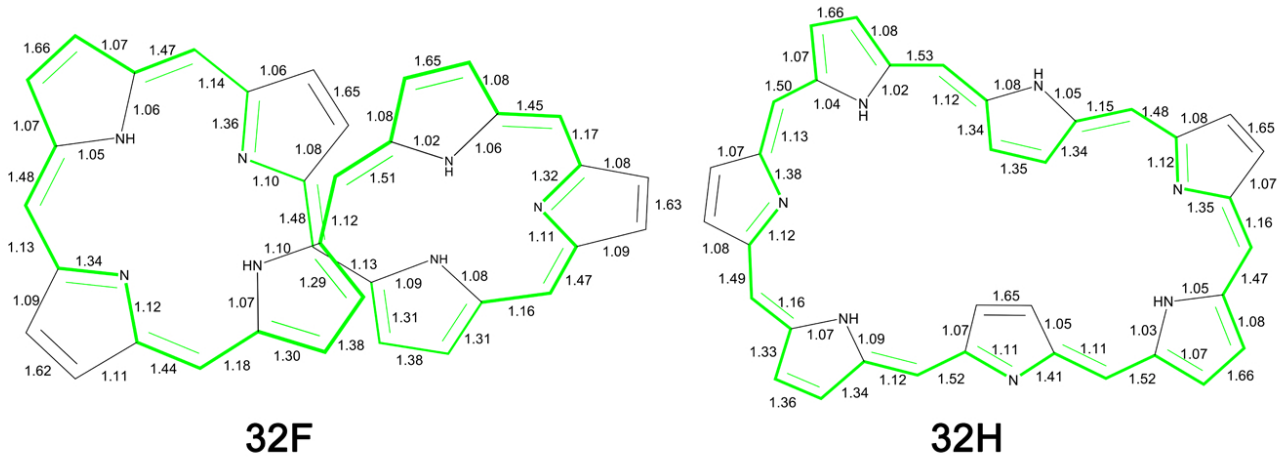

Figure S15: Delocalization indices (DIs) for **32F** and **32H** macrocycles computed at the CAM-B3LYP/6-311G(d,p) level of theory. The main conjugation pathway is depicted with bold bonds.

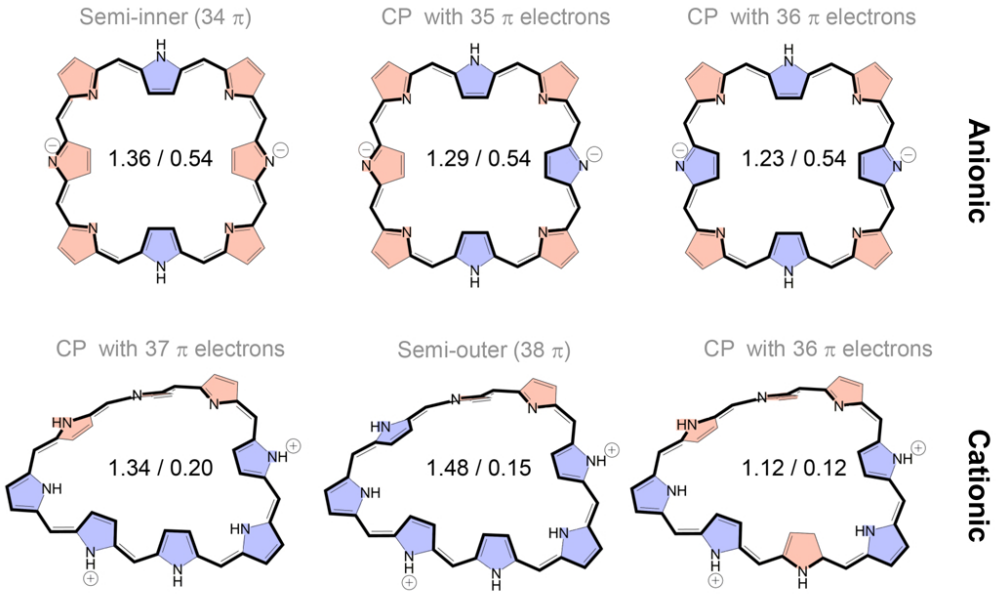

Figure S16: Illustration of the most delocalized pathways in $\mathbf{36H}_a^{2-}$ and $\mathbf{36M}_b^{2+}$.

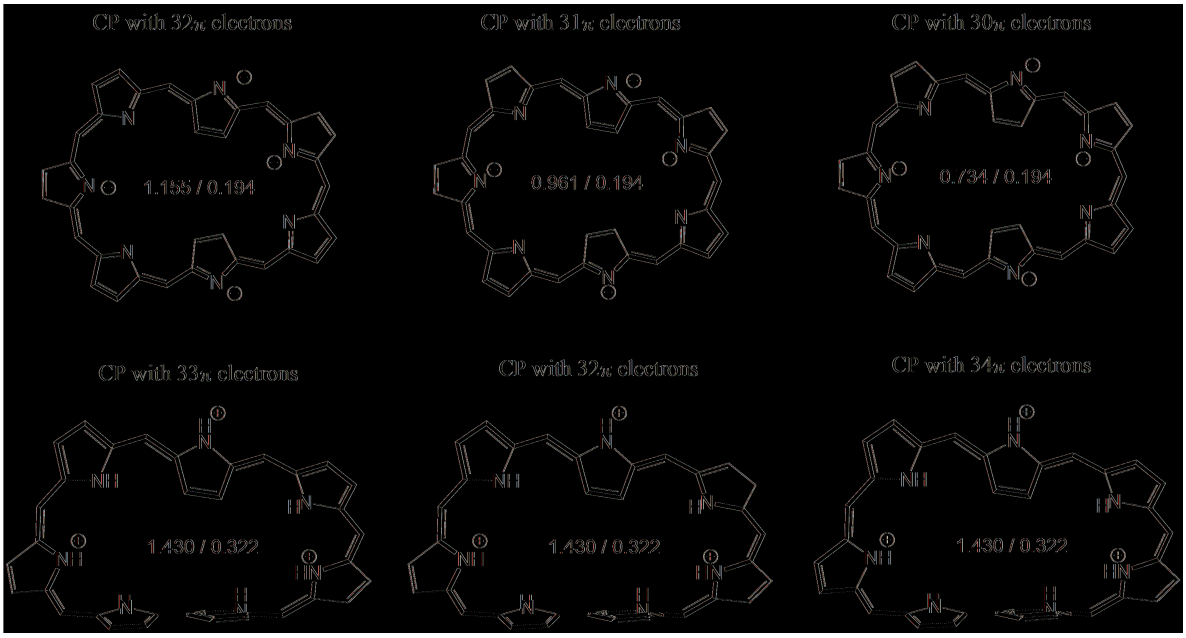

Figure S17: Illustration of the most delocalized pathways in $\mathbf{32H}^{4-}$ and $\mathbf{32M}^{3+}$.

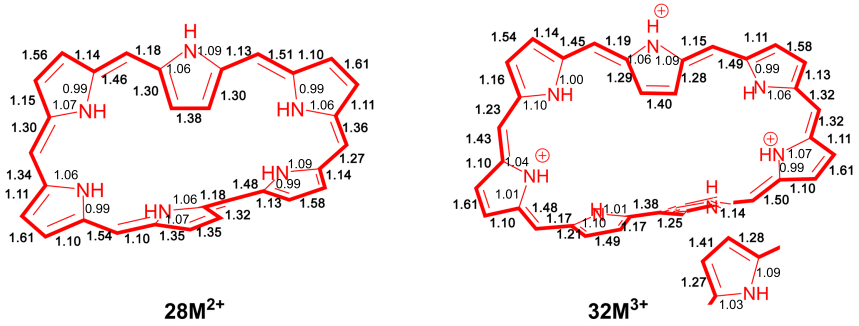

Figure S18: Delocalization indices (DIs) for $\mathbf{28M}^{2+}$ and $\mathbf{32M}^{3+}$ macrocycles computed at the CAM-B3LYP/6-311G(d,p) level of theory. The main conjugation pathway is depicted with bold bonds.

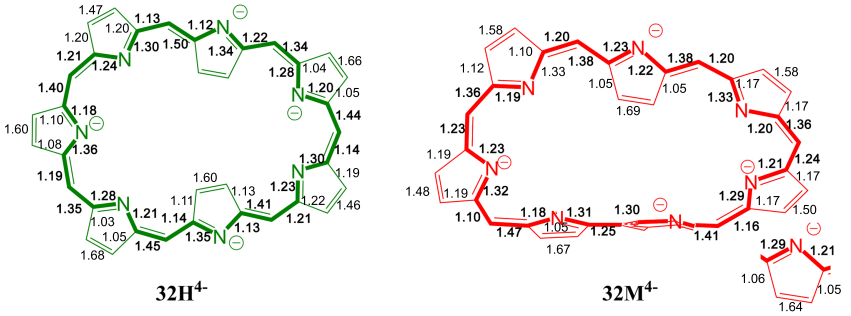

Figure S19: Delocalization indices (DIs) for $\mathbf{32H}^{4-}$ and $\mathbf{32M}^{4-}$ macrocycles computed at the CAM-B3LYP/6-311G(d,p) level of theory. The main conjugation pathway is depicted with bold bonds.

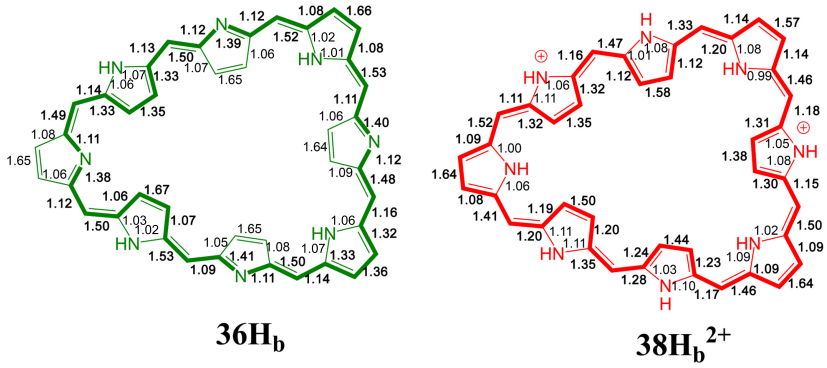

36H$_b$ **38H$_b^{2+}$**

Figure S20: Delocalization indices (DIs) for **36H**$_b$ and **38H**$_b^{2+}$ macrocycles computed at the CAM-B3LYP/6-311G(d,p) level of theory. The main conjugation pathway is depicted with bold bonds.

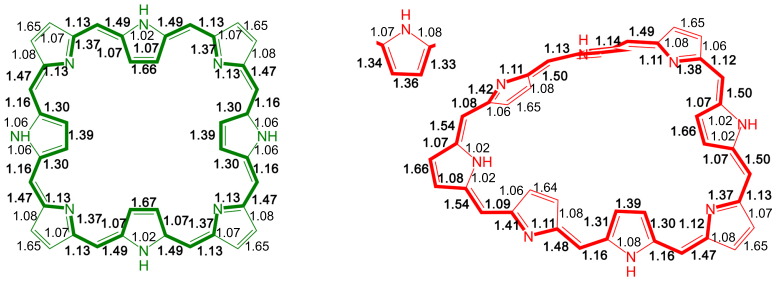

36H$_a$ **36M$_b$**

Figure S21: Delocalization indices (DIs) for **36H**$_a$ and **36M**$_b$ macrocycles computed at the CAM-B3LYP/6-311G(d,p) level of theory. The main conjugation pathway is depicted with bold bonds.